Synthesis and preliminary radiopharmacological characterisation of an ^{11}C-labelled azadipeptide nitrile as potential PET tracer for imaging of cysteine cathepsins

Laube, M.; Frizler, M.; Wodtke, R.; Neuber, C.; Belter, B.; Kniess, T.; Bachmann, M.; Gütschow, M.; Pietzsch, J.; Löser, R.;

Originally published:

March 2019

Journal of Labelled Compounds and Radiopharmaceuticals 62(2019)8, 448-459

DOI: https://doi.org/10.1002/jlcr.3729

Synthesis and preliminary radiopharmacological characterisation of an ^{11}C-labelled azadipeptide nitrile as potential PET tracer for imaging of cysteine cathepsins**

Markus Laube[1], Maxim Frizler[2,4], Robert Wodtke[1], Christin Neuber[1], Birgit Belter[1], Torsten Kniess[1], Michael Bachmann[1], Michael Gütschow[2], Jens Pietzsch[1,3], Reik Löser[1,3,*]

[1]*Helmholtz-Zentrum Dresden-Rossendorf, Institute of Radiopharmaceutical Cancer Research, Bautzner Landstraße 400, 01328 Dresden, Germany*
[2]*Pharmaceutical Institute, Pharmaceutical Chemistry I, Rheinische Friedrich-Wilhelms-Universität, An der Immenburg 4, D-53121 Bonn, Germany*
[3]*Faculty of Chemistry and Food Chemistry, School of Science, Technische Universität Dresden, Mommsenstraße 4, 01062 Dresden, Germany*
[4]*present address: Federal Institute for Drugs and Medical Devices (BfArM), Kurt-Georg-Kiesinger-Allee 3, 53175 Bonn, Germany*

Abstract

An *O*-methyltyrosine-containing azadipeptide nitrile was synthesised and investigated for its inhibitory activity towards cathepsins L, S, K and B. Labelling with carbon-11 was accomplished by reaction of the corresponding phenolic precursor with [^{11}C]methyl iodide starting from cyclotron-produced [^{11}C]methane. Radiopharmacological evaluation of the resulting radiotracer in a mouse xenograft model derived from a mammary tumour cell line by small animal PET imaging indicates tumour targeting with complex pharmacokinetics. Radiotracer uptake in the tumour region was considerably lower under treatment with the non-radioactive reference compound and the epoxide-based irreversible cysteine cathepsin inhibitor E64. The in vivo behaviour observed for this radiotracer largely confirms that of the corresponding ^{18}F-fluoroethylated analogue and suggests the limited suitability of azadipeptide nitriles for the imaging of tumour-associated cysteine cathepsins.

**Email: r.loeser@hzdr.de*
***Dedicated to Prof. Dr. Jörg Steinbach on the occasion of his retirement in appreciation of his thoughtful and selfless leadership.*

1. Introduction

Cysteine cathepsins are important players in various human disease processes[1,2] including diabetes,[3] obesity,[4] inflammatory[5] and autoimmune disorders,[6] neurodegenerative,[7] cardiovascular[8] and fibrotic diseases[9] and – most evidently – cancer.[10-13] In the last two decades these enzymes attracted a lot of interest as potential drug targets[14-17] and more recently their imaging in the physiological context in vivo has come into focus.[18,19]

With regards to molecular imaging of cysteine cathepsins by positron emission tomography (PET), inhibitor-based radiotracers labelled with carbon-11,[20,21] fluorine-18,[22] copper-64[23,24] and gallium-68[25] have been reported (Figure 1). The employed inhibitor chemotypes cover irreversibly acting acyloxymethyl ketones (e.g. [^{64}Cu]**A**[23] and [^{68}Ga]**B**[25]) and nitriles, which interact with the enzymes in a reversible-covalent manner (e.g. [^{11}C]**C**[20], [^{11}C]**D**[21] and [^{18}F]**E**[22]). The latter mentioned radiotracer is based on the azadipeptide nitrile core structure. Inhibitors of this type have been proven to interact with cysteine cathepsins with high affinity and to exhibit stability towards degradation by other proteolytic enzymes.[26] The radiopharmacological characterisation of this radiotracer in a mouse xenograft model of human lung cancer has revealed that its pharmacokinetic behaviour is largely determined by its uncatalysed reaction with glutathione, even though a target-mediated tumour uptake was discernible.[22] Despite fluorine-18 can be considered as the optimal PET nuclide concerning positron energy,[27] labelling with carbon-11 is highly attractive. This is due to the fact that it requires only minimal structural changes of lead compounds and even authentic labelling can be achieved with this radionuclide.[28-32] In this regard it is advantageous that various functional groups containing carbon in different oxidation states can be synthesised starting from cyclotron-produced [^{11}C]methane and [^{11}C]carbon dioxide.[33-37] However, the most often applied routes for introduction of carbon-11 involve ^{11}C-methylation of nucleophilic functional groups using [^{11}C]methyl iodide or [^{11}C]methyl triflate.[38,39] Moreover, ^{11}C-methylation is considered to be complementary to ^{18}F-fluoroethylation, as both radiolabelling approaches can be used on identical precursors and result in similar degrees of structural alteration and therefore in similar physicochemical properties of the tracer compounds.[40] Owing to the short half-life of 20.4 min, ^{11}C-labelled compounds allow for repeated imaging studies in terms of test-retest paradigms.[41,42]

Motivated by the advantages of carbon-11 mentioned above, we envisaged the ^{11}C-labelling of an azadipeptide nitrile. In particular, we report on the ^{11}C-methylation of the phenolic precursor that was previously employed in the synthesis of [^{18}F]**E** (Figure 1) by ^{18}F-fluoroethylation,[22] and its preliminary radiopharmacological characterisation by dynamic small animal PET imaging using a mouse xenograft model of mammary carcinoma. Therefore, the synthesis of the complementary ^{11}C-based radiotracer to [^{18}F]**E** was established within this study and its radiopharmacological properties are discussed in comparison to those of its ^{18}F-labelled counterpart.

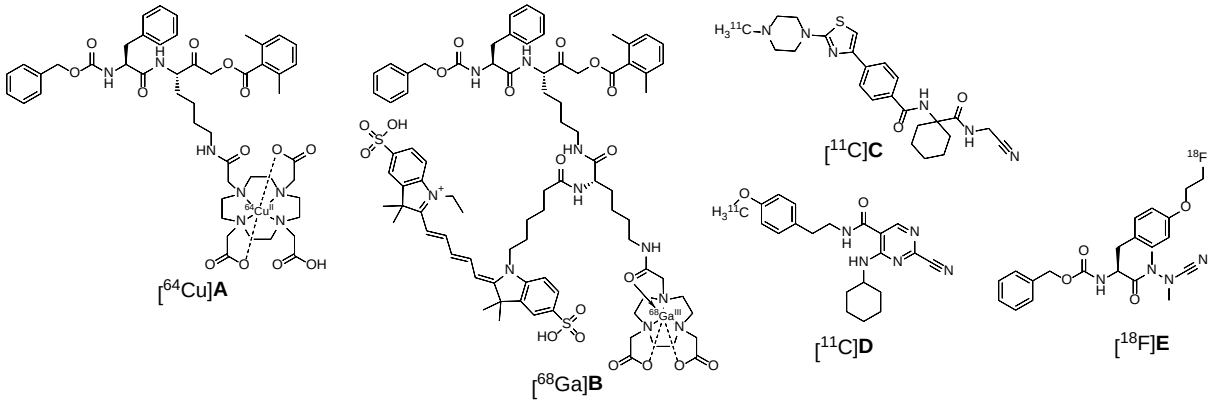

Figure 1: Selected inhibitor-based radiotracers for PET imaging of cysteine cathepsins.

2. Experimental

2.1. General remarks

All commercial reagents and solvents were used without further purification unless otherwise specified. Nuclear magnetic resonance spectra were recorded on a Bruker Avance 500 spectrometer at 25 °C. NMR chemical shifts were referenced with the residual solvent resonances relative to tetramethylsilane (TMS). Electrospray ionisation (ESI) mass spectra were obtained on a Waters (Milford, MA, USA) Xevo TQ-S mass spectrometer driven by the Mass Lynx software. Preparative column chromatography was carried out using Merck silica gel (mesh size 230–400 ASTM) with solvent mixtures as specified for the particular compounds. Thin-layer chromatography (TLC) was performed on Merck silica gel F-254 aluminium plates with visualisation under UV light (254 nm). Radio-TLC was conducted the same way with petroleum ether/ethyl acetate 1:2 as eluent. Radioactive spots were visualised using the Fujix Bas2000 TR radioluminography system. The identity of the radioactive spots was proven with the corresponding non-radioactive reference compounds that were spotted with radioactivity after visualisation under UV.
Analytical radio-HPLC was performed on a Luna C18 5 µm column (Phenomenex, 250×4.6 mm) using 50 % CH_3CN/water containing 0.1 % trifluoroacetic acid as isocratic eluent pumped by a Merck Hitachi L7100 gradient pump at a flow rate of 1 mL/min through a Jasco DG2080 4-line degasser with UV detection by a Merck Hitachi L7450 diode array detector and γ detection by a Raytest GABI detector. The system was operated by the D-7000 HSM software using a Merck Hitachi D7000 interface.

2.2. Synthesis of non-radioactive reference compound benzyl (*S*)-(1-(2-cyano-1,2-dimethylhydrazineyl)-3-(4-methoxyphenyl)-1-oxopropan-2-yl)carbamate (2)

Compound **1** (2.44 g, 6.38 mmol; prepared as reported)[43] was dissolved in dry DMF (20 mL) and cooled to -10 °C. The resulting solution was treated with sodium hydride (280 mg (60% in mineral oil), 7.00 mmol) and stirred at -10 °C for 30 min. Methyl iodide (1.80 g, 0.79 mL, 12.7 mmol) was added and the reaction solution was slowly warmed to room temperature and stirred for 24 h at room temperature. The solvent was removed under reduced pressure, the resulting residue was suspended in H_2O (30 mL), and extracted with ethyl acetate (3×30 mL). The combined organic layers were washed with H_2O (30 mL) and brine (30 mL), dried (Na_2SO_4) and evaporated. The crude product was purified by column chromatography using ethyl acetate/petroleum ether (1:1) as eluent to obtain **2** as a colorless oil (1.30 g, 51%). ^{1}H NMR (500 MHz, DMSO-d_6) δ 2.73–2.81 (m, 2H, CHCH_2), 2.96, 3.08, 3.12, 3.22 (4 × s, 6H, 2 × NCH_3), 3.71 (s, 3H, OCH_3), 4.67 (br s, 1H, NHC*H*CO), 4.95 (s, 2H, CH_2O), 6.85–7.34 (m, 9H, H_{arom}), 7.78–7.87 (m, 1H, N*H*CHCO), ^{13}C NMR (125 MHz, DMSO-d_6) δ 30.27, 30.59, 35.66, 36.07, 40.28, 40.48, (2 × NCH_3, CH*C*H_2), 52.92, 53.40 (NH*C*HCO), 55.12 (OCH_3), 65.63 (CH_2O), 113.94 (C_{arom}), 114.22 (CN), 127.75, 127.91, 128.42, 129.41, 130.20, 130.41, 136.92 (C_{arom}), 155.87, 156.29 (OCON), 158.23 (C_{arom}), 173.53 (NHCH*C*O). MS (ESI+) m/z calculated: 396.18, found: 397.1 $[M+H]^+$

2.3. Enzyme inhibition assay

Kinetic inhibition assays for compound **2** on cathepsins L, S, B and K were performed as described previously.[43]

2.4. Radiosynthesis of (*S*)-(1-(2-cyano-1,2-dimethylhydrazineyl)-3-(4-[*methyl*-^{11}C]methoxyphenyl)-1-oxopropan-2-yl)carbamate ([^{11}C]2)

[^{11}C]CH_4 was produced by the ^{14}N(p,α)^{11}C nuclear reaction on a CYCLONE 18/9 cyclotron (IBA) by irradiation of nitrogen gas containing 10% hydrogen in an aluminium target containment. Synthesis of [^{11}C]CH_3I and subsequent conversion to [^{11}C]**2** followed by purification of the product was performed fully automated and remotely controlled in a TracerLab $FX_{C\text{-}Pro}$ (GE) synthesizer.
Compound **1** (1 mg, 2.61 µmol) was dissolved in dry DMF (250 µL). A solution of NaH (60% in mineral oil) in dry DMF at a concentration of 0.1 M was freshly prepared prior to every radiosynthesis and 26.1 µL of this solution were added to the solution of **1**. The resulting mixture was transferred into the reactor vial under nitrogen. [^{11}C]CH_4 was separated from the target gas by trapping on GraphPac

GC (60/80 mesh, Alltech) at -140°C and purging with helium. By heating to 80 °C, [^{11}C]CH_4 was released from the trapping material and processed in the iodine reactor at 720 °C in repetitive circulation. The synthesised [^{11}C]CH_3I was trapped during the synthesis on Porapak Q (50-80 mesh, Alltech) at room temperature. At the end of this process, [^{11}C]CH_3I was released from the Porapak trap by heating to 190 °C and transferred in a stream of helium into the reaction vessel at a temperature of -20 °C. After completion of the transfer, the reaction vessel was sealed and heated at 80 °C for 2 min. The reactor was cooled to 40 °C, 700 µL of HPLC eluent (CH_3CN/ 0.1% CF_3COOH in H_2O 1/1 (v/v)) were added to the reaction mixture and the resulting solution was transferred onto the semi-preparative HPLC column (Phenomenex® Gemini 5µ C18 100Å, 250×10 mm; guard column: SecurityGuard™ SemiPrep C18). HPLC purification was performed at a flow of 4 mL/min delivered by a HPLC pump (Synkam S1021 Solvent Delivery System) equipped with degasser (Degasys DG-1310) under observation the UV signal at 254 nm (Knauer, UV-Detector K-2001) and the radioactivity signal. The product-containing fraction was collected and diluted into water (50 mL). The resulting mixture was loaded onto a solid phase extraction cartridge (Lichrolut RP18E 200 mg; preconditioned with ethanol and water). The cartridge was washed with water (10 mL) and eluted with absolute ethanol (0.5 mL). The eluted radiotracer solution was further concentrated by heating in a N_2 stream. For product analysis and determination of the molar activity of [^{11}C]**2**, a definite activity (around 5 MBq) was subjected to analytical radio-HPLC. The trace profile for 215 nm was retrieved from the recorded DAD data and the area under the curve was determined for the product. The molar amount was calculated from a calibration line obtained from HPLC analyses of **2** in masses ranging from 0.01 to 1 µg on column.

The distribution coefficient log $D_{7.4}$, which is equal to log P due to the absence of an ionisable group in the tracer compound, was determined by adding 1 µL of the ethanolic solution of [^{11}C]**2** to a mixture of n-octanol (600 µL; presaturated with phosphate-buffered saline) and phosphate-buffered saline (600 µL; presaturated with n-octanol). The resulting mixture was vortexed for 5 min at room temperature. For phase separation, the tube was shortly centrifuged and 400 µL of the organic layer were added to phosphate-buffered saline (400 µL; presaturated with n-octanol) and the resulting mixture was again vortexed for 5 min. Aliquots (250 µL) of each phase were transferred to separate tubes; transfer of the aqueous phase requires special care according to Linclau et al.[44] The activity of separated layers were measured in a well counter and each corrected by subtracting the background activity. The activities were decay-corrected considering the time differences between the measurements of the corresponding different phases. The distribution coefficient was calculated by log $D_{7.4}$=log[count rate(octanol phase)/count rate(aqueous phase)]. A value of 2.38±0.06 (mean±SEM) was determined form three distinct experiments starting from the identical radiotracer solution.

The reaction of [^{11}C]**2** with glutathione was investigated by adding 2 µL of radiotracer solution (1.5 MBq) to 200 µL of 5 mM glutathione in PBS. The resulting mixture was incubated at 37°C and aliquots of 25 µL were subjected to analysis by radio-HPLC after 2 and 40 min.

2.5. PET imaging experiments

Animal experiments were carried out in accordance to the guidelines of the German Regulations for Animal Welfare. The protocol was approved by the local Ethical Committee for Animal Experiments (reference number 24-9168.11-4/2012-1). This study was designed as an orientation survey.

PET experiments were performed in female nude mice (NMRI Foxn1$^{nu/nu}$; body weight 27.2±2.5 g) bearing MDA-MB-231 STn-Luc human mammary adenocarcinoma[45] using 7.8±2.2 MBq of [^{11}C]**2** following the protocols published elsewhere with some minor modifications.[44,46] In brief, PET experiments using dedicated PET/CT scanner for small animals (NanoScan PET/CT scanner, Mediso) were performed when tumours reached a diameter of about 7-9 mm. General anesthesia of mice was induced and maintained by inhalation of 10% desflurane in 30% oxygen/air. PET acquisition was started 10 s before intravenous (i.v.) infusion of the radiotracer through a needle catheter into a lateral tail vein and emission data were acquired continuously for 60 min. For blocking experiments, mice were simultaneously injected intravenously with non-radioactive **2** (26.6 mg/kg body weight; in 100 µL saline with 10% DMSO), the broad-band cysteine peptidase inhibitor E64 (9.3 mg/kg body weight; in 100 µL saline) or intraperitoneally 30 min before the radiotracer with the glutathione *S*-reactive agent diethyl maleate (DEM; 567 mg/kg body weight; in 200 µL sunflower oil). Acquired data were sorted into 32 time frames and reconstructed as described elsewhere.[47] Image volume data were

analysed by ROVER software (ABX GmbH). Three-dimensional regions of interest (ROI) were determined within masks around the tumours or different organs by thresholding PET data within these masks. ROI time activity curves (TAC) and SUV (SUV = activity concentration in tissue × body weight / injected dose) are given as mean ± SD (control: n=6) or single records (blocked; **2**, n=2, E64, n=2; DEM, n=1).

3. Results and Discussion

To allow for a facile attachment of carbon-11 to the azadipeptide nitrile core structure, we utilised the azadipeptide nitrile **1**, which itself represents a potent cathepsin inhibitor[43] and which was previously successfully employed by us as labelling precursor for ^{18}F-fluoroethylation towards [^{18}F]**E**.[22] Compound **1**, bearing tyrosine in position P^2, was converted into the reference compound **2** by methylation of its phenolic hydroxyl group according to Scheme 1.

Kinetic evaluation of azadipetide nitrile **2** towards inhibition of the oncologically relevant cathepsins L, S, K, and B was performed using continuous enzyme activity assays with appropriate fluorogenic or chromogenic substrates. The resulting parameters included in Table 1 indicate that the extraordinary inhibitory potency of the parent compound **1**[43] is largely retained upon *O*-methylation of its tyrosine side chain as realised in compound **2**. However, according to the equilibrium inhibition constants, the affinity of **2** to cathepsin B is diminished by one order of magnitude, even though it is still in the single-digit nanomolar range. This loss in inhibitory activity can be clearly attributed to an increased k_{off} value compared to **1**, which represents the rate constant describing the disintegration of the enzyme-inhibitor complex into unbound inhibitor and free enzyme. As for the parent compound **1**, the K_i values of **2** towards the cathepsins L, S and K are in the subnanomolar range. Notably, different to fluoroethylation, the affinity of **1** for cathepsin K slightly increased upon methylation, which is reflected in increased association (k_{on}) and decreased dissociation (k_{off}) rate constants.

Table 1. Inhibition of thiol-dependent cathepsins by the azadipeptide nitriles **1** and **2**. For comparison, the inhibitory activities of compound **E** were included as published in ref.[22]

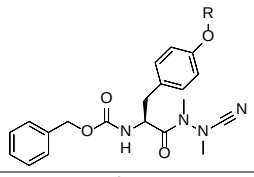

cathepsin		**1 (R=H)***	**2 (R=CH$_3$)**	**E (R=(CH$_2$)$_2$F)****
L	K_i (nM)	0.36±0.03	0.68±0.06	0.73±0.06
	k_{on} (10^3 $M^{-1}s^{-1}$)	4200±100	1200±500	930±100
	k_{off} (10^{-3} s^{-1})	1.5±0.1	0.82±0.35	0.68±0.09
S	K_i (nM)	0.86±0.02	0.46±0.05	0.79±0.06
	k_{on} (10^3 $M^{-1}s^{-1}$)	500±30	990±400	560±100
	k_{off} (10^{-3} s^{-1})	0.43±0.03	0.46±0.19	0.44±0.09
B	K_i (nM)	0.38±0.03	2.2±0.4	2.4±0.1
	k_{on} (10^3 $M^{-1}s^{-1}$)	79±22	180±10	190±10
	k_{off} (10^{-3} s^{-1})	0.030±0.009	0.40±0.08	0.46±0.03
K	K_i (nM)	0.16±0.01	0.085±0.01	0.17±0.01
	k_{on} (10^3 $M^{-1}s^{-1}$)	320±20	480±40	210±50
	k_{off} (10^{-3} s^{-1})	0.051±0.005	0.041±0.006	0.036±0.009

*values taken from ref.[43], **values taken from ref.[22]

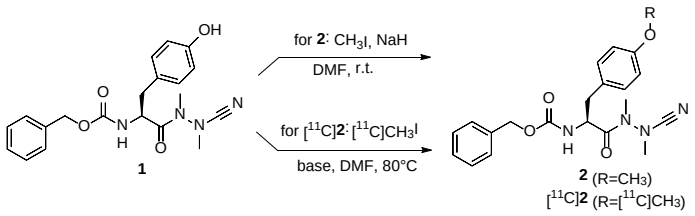

Scheme 1. Synthesis of the side-chain *O*-methylated azadipeptide nitrile **2** and its ^{11}C-labelled version [^{11}C]**2**. Synthesis of [^{11}C]**2** was optimised regarding the base as shown in Figure 2.

Labelling of azadipeptide nitrile **2** with carbon-11 was performed in orientation to the synthesis of the non-radioactive reference compound by conversion of **1** with [^{11}C]methyl iodide. For this, the ^{14}N(p,α)^{11}C reaction, performed by irradiating nitrogen gas containing 10 % of hydrogen with a cyclotron, was utilised to generate [^{11}C]methane as starting material for the following automated radiosynthetic process. Using the commercially available TracerLab FX$_{C\text{-}Pro}$ synthesis module (Figure 3A), [^{11}C]methane was passed in repetitive circulations through an iodine reactor to produce the labelling agent [^{11}C]methyl iodide by the gas-phase method. Subsequently, conversion of **1** with [^{11}C]methyl iodide was attempted using DMF and sodium hydride as base creating [^{11}C]**2** in 35% non-isolated radiochemical yield as determined by radio-HPLC. Employment of sodium hydride in equimolar concentration to the precursor **1** was superior over aqueous sodium hydroxide or DBU as alternative bases (Figure 2). This result can be rationalised by considering that quantitative and irreversible deprotonation of the phenolic hydroxyl group can only be caused by sodium hydride, whereas reversible acid-base equilibria are attained in the case of the other two bases. Surprisingly, the least favourable outcome of the reaction was observed when DBU was used as base, which might be due to the competing reaction of DBU with [^{11}C]methyl iodide, which has been observed for unlabelled methyl iodide.[48] Contrary to the results observed for the ^{11}C-methylation of **1**, DBU was successfully employed as base in other radiotracer syntheses with [^{11}C]methyl iodide.[49]

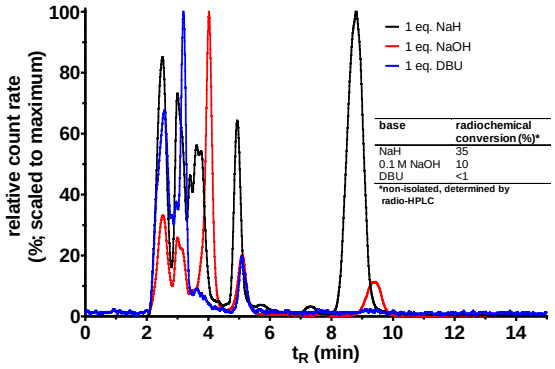

Figure 2: Influence of the kind of base on the conversion of **1** to [^{11}C]**2** with [^{11}C]methyl iodide. Shown are the radio-HPLC chromatograms of the reaction mixtures in the presence of various bases. The inset table shows the radiochemical yields as determined by radio-HPLC analysis. Retention time of [^{11}C]**2** varied between 8.80-10.04 min in the employed HPLC system.

Separation of [^{11}C]**2** from unconverted **1** and ^{11}C-labelled side products was achieved by subjecting the reaction mixture to semi-preparative HPLC using 50 % acetonitrile/water containing 0.1 % trifluoroacetic acid as isocratic eluent (Figure 3B). The product-containing eluate was separated from the HPLC eluent and concentrated by solid-phase extraction and subsequent elution with ethanol. The elaborated procedure allowed for a reliable automated synthesis of the ^{11}C-labelled azadipeptide nitrile [^{11}C]**2** in good radiochemical yields, radiochemical purities and molar activities (Figure 4 and Table 2). The activity range of [^{11}C]**2** obtained from varying activities of [^{11}C]methane is shown in Table 2. In a typical radiosynthesis, 388 MBq of [^{11}C]**2** were obtained from 10.8 GBq of cyclotron-produced [^{11}C]methane via 5.5 GBq of intermediary [^{11}C]methyl iodide within a synthesis time of 41 min, which corresponds to a radiochemical yield of 14.5 %. The radiochemical purities of the product determined by radio-TLC and radio-HPLC were greater than 95 or 97 %, respectively (Table 2). The range of

molar activities for [^{11}C]**2** (Table 2) was acceptable for small animal PET experiments and was comparable to that of other carbon-11-based radiotracers obtained via gas phase-produced [^{11}C]methyl iodide.[50,51]

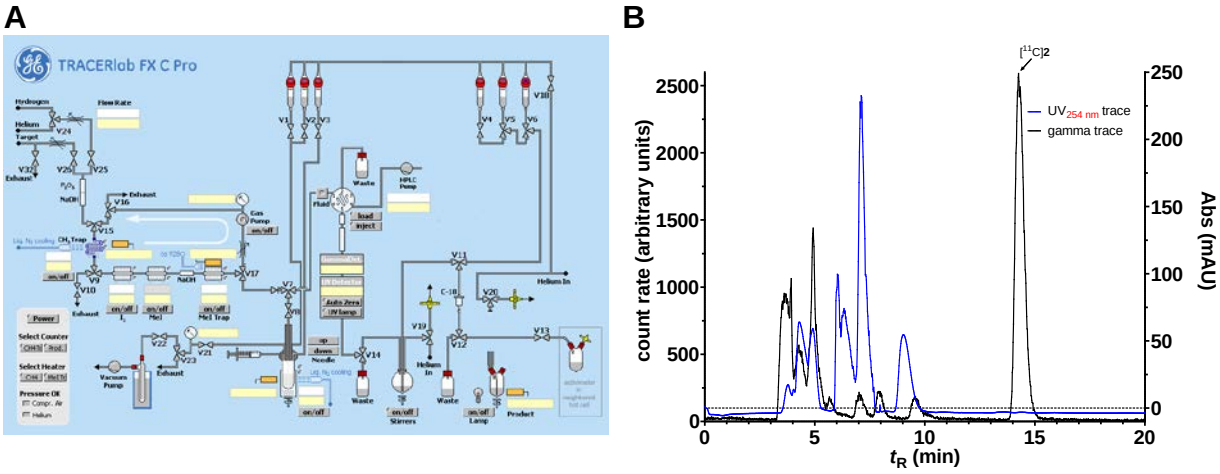

Figure 3: Configuration of the Tracerlab FX$_{C\text{-}Pro}$ synthesis module (**A**) and representative semi-preparative radio-HPLC chromatogram for purification of [^{11}C]**2** (**B**). blue: UV-channel, black: γ-channel; stationary phase: phenomenex gemini C18, 250×10 mm, 5 µm, 100 Å, eluent: $CH_3CN/H_2O/CF_3CO_2H$ 1:1:0.1 (4 mL/min).

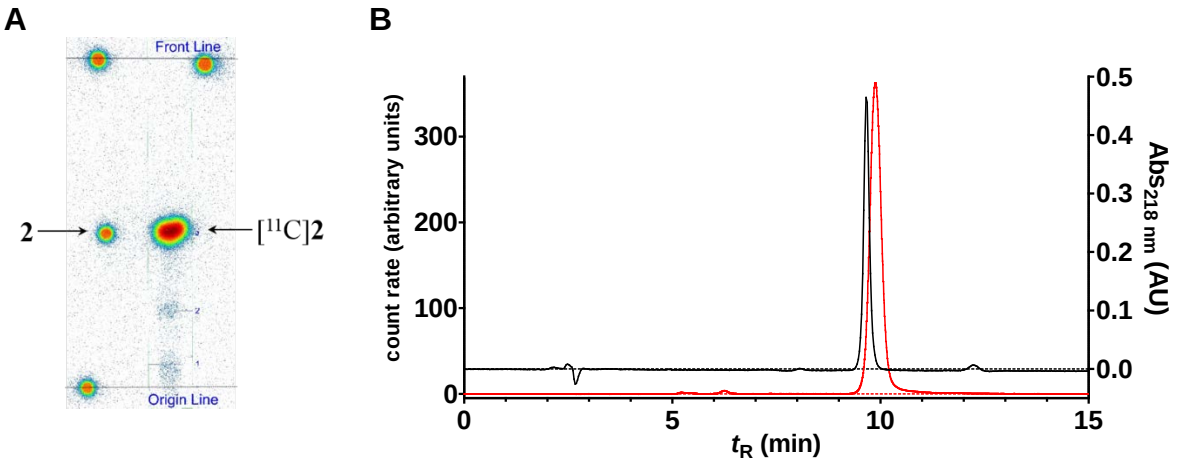

Figure 4: Proof of identity and radiochemical purity of [^{11}C]**2** by analytical radio-chromatography. A) radio-TLC of the final product (right) and the reference compound (left) spotted with radioactivity after UV -visualisation, B) radio-HPLC (red trace) overlaid with the HPLC chromatogram of **2** monitored at 218 nm.

Table 2: Radiochemical parameters for the synthesis of [^{11}C]**2**

parameter		**range**	**mean±SEM**	***n***
[^{11}C]CH_4 starting activity (GBq)		7.0-14.3		10
[^{11}C]CH_3I intermediate activity (GBq)		2.5-6.1		10
product activity (MBq)		126-526		10
radiochemical yield (d.c.; %)		8.2-21.6	13.6±1.6	10
radiochemical purity (%)	radio-HPLC	97.5-99.3	98.7±0.2	10
	radio-TLC	95.8-99.1	97.3±0.5	9
molar activity (GBq/µmol)		29.9-81.4	62.6±8.1	6
synthesis time (min)		37-52	44.1±1.2	10

Using the classical shake-flask method, a partition coefficient (log P) of 2.38 was determined for azadipeptide nitrile [^{11}C]**2**. This value is comparable to log P of its ^{18}F-fluoroethylated analogue

(radiotracer **E** in Figure 1), which was determined to be 2.30.[22] This result is in accordance to the observation of similar lipophilicities for other ^{11}C-methylated/^{18}F-fluoroethylated radiotracer pairs.[52]

Based on the successfully established radiosynthesis of [^{11}C]**2**, its radiopharmacological investigation in nude mice bearing tumour xenografts derived from MDA-MB-231 STn-Luc cells using PET imaging was enabled. The expression of the oncologically relevant cysteine cathepsins B, L, and S in this aggressive triple-negative human breast cancer cell line was confirmed by several studies.[53-56] The PET images are shown in Figure 5A and Figure 6A. The rescaled images indicate that the C-11 activity is distributed over the entire organism, even though the tumour tissue is distinguishable. Hence, the pharmacokinetic behaviour of [^{11}C]**2** largely resembles that of its ^{18}F-fluoroethylated analogue [^{18}F]**E**, whose biodistribution pattern is mainly determined by its long blood residence. In the case of [^{18}F]**E**, the slow blood clearance has been attributed to its spontaneous reaction with glutathione, which results in the retention of the resulting conjugate in the erythrocytes. Nevertheless, a considerable fraction of the original unmodified radiotracer was still detectable in blood plasma at 60 min p.i.[22] Conjugate formation between [^{11}C]**2** has been confirmed by incubation of the radiotracer with glutathione at a concentration of 5 mM (Figure 7).

The time-activity curves shown in Figure 8 indicate that the tumour uptake of [^{11}C]**2** is low ($SUV_{tumour,\ 55\ min} < 0.1$; unblocked; n=6) but slightly higher than in muscle tissue with a mean tumour-to-muscle ratio of 1.37±0.51 for the investigation time. As for [^{18}F]**E**, the tumour-to-blood ratio of [^{11}C]**2** lies in favour to blood but is smaller than that of its ^{18}F-fluoroethylated counterpart (0.09 for [^{11}C]**2** *versus* 0.49 for [^{18}F]**E** at 55 min p.i.).[22]

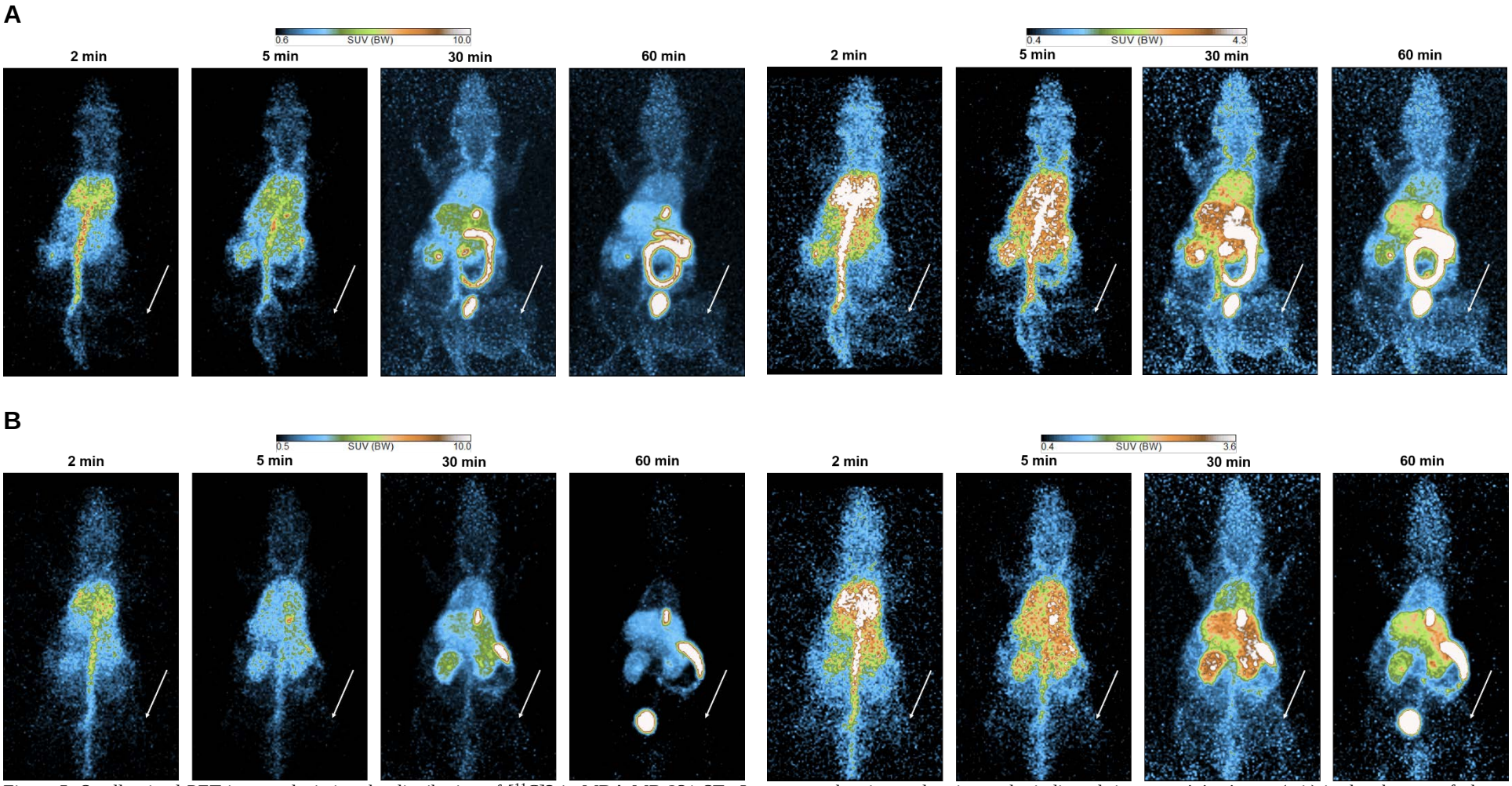

Figure 5: Small animal PET images depicting the distribution of [^{11}C]**2** in MDA-MB-231 STn-Luc tumour-bearing nude mice at the indicated time *post injectionem* (p.i.) in the absence of pharmacological blockade (**A**) and treated with unlabelled **2** (26.6 mg/kg) (**B**). Shown are maximum intensity projections scaled according to maximum (left panels each) and rescaled mode (right panels each). The location of the tumour tissue is indicated by an arrow.

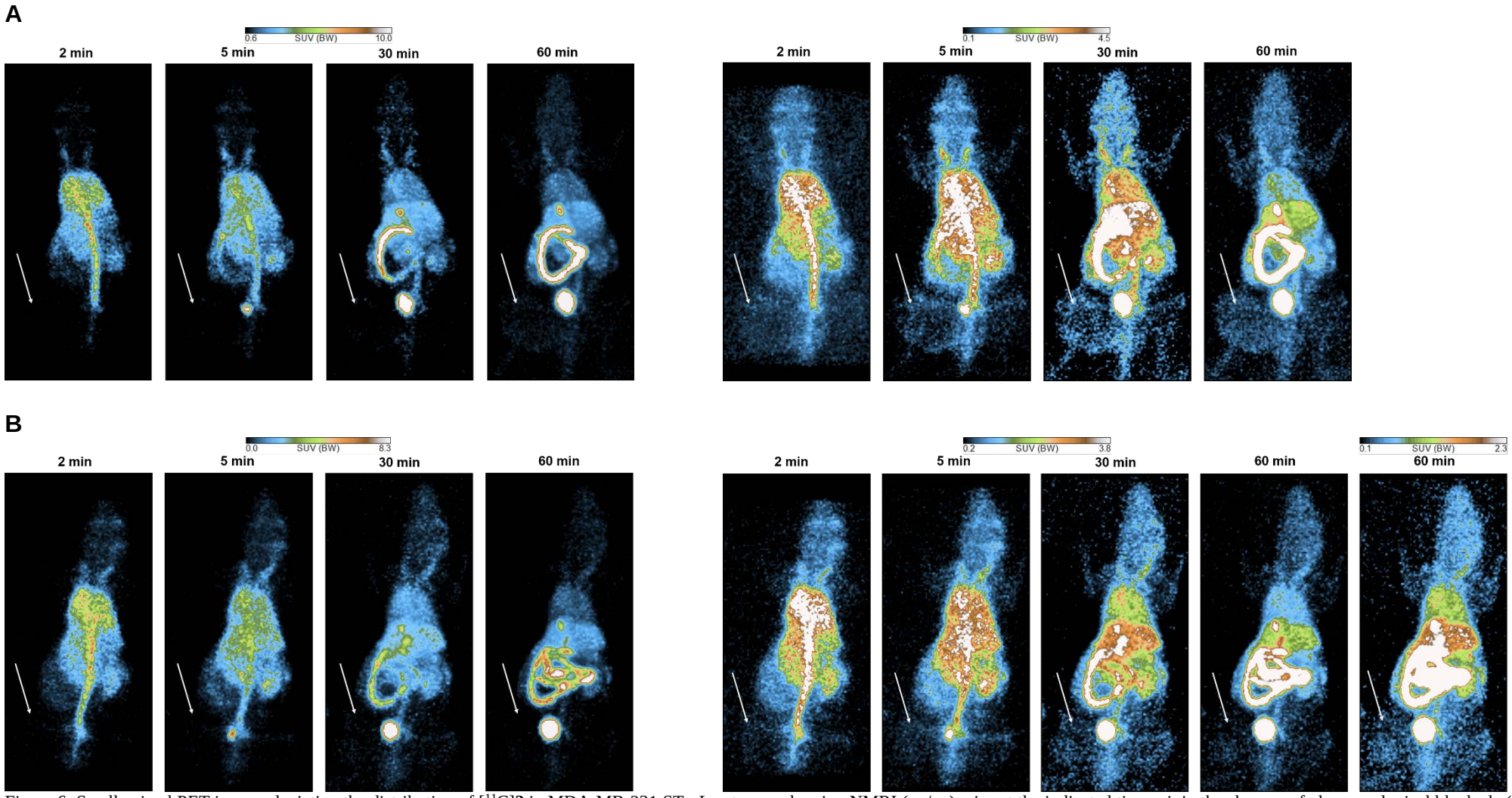

Figure 6: Small animal PET images depicting the distribution of [^{11}C]**2** in MDA-MB-231 STn-Luc tumour-bearing NMRI (nu/nu) mice at the indicated time p.i. in the absence of pharmacological blockade (**A**) and treated with E64 (9.3 mg/kg) (**B**). Shown are maximum intensity projections scaled according to maximum (left panels each) and rescaled mode (right panels each). The location of the tumour tissue is indicated by an arrow.

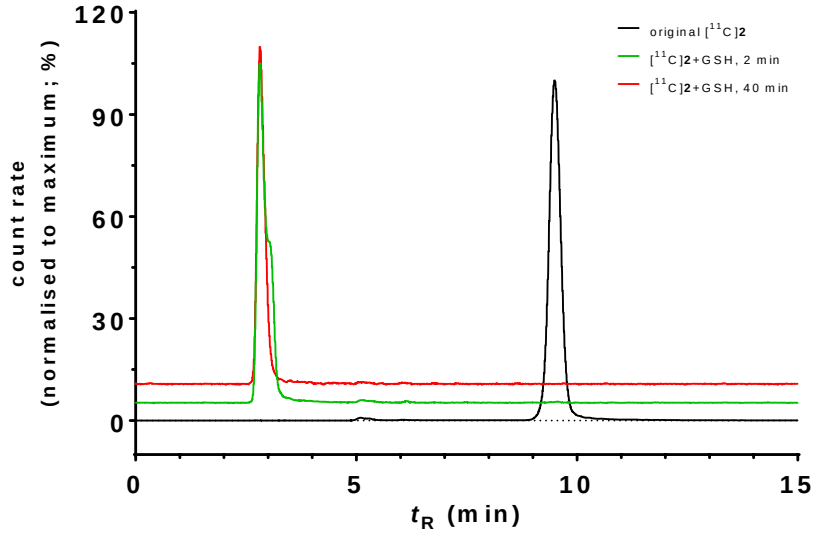

Figure 7: Conjugate formation between azadipeptide nitrile [^{11}C]**2** and glutathione as demonstrated by radio-HPLC. For better visualisation, radio-HPLC chromatograms for 2 and 40 min were shifted 5 and 10%, respectively, at the ordinate.

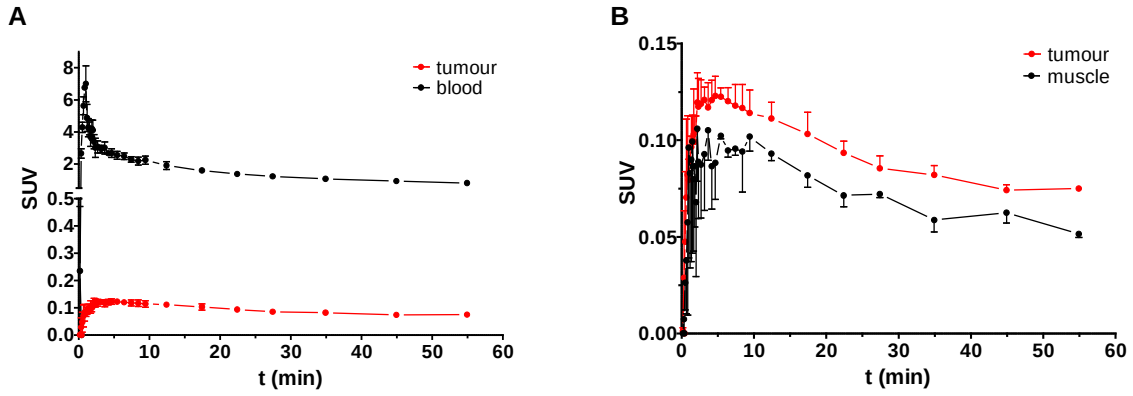

Figure 8: Time-activity curves for [^{11}C]**2** in the tumour region in comparison to muscle and blood.

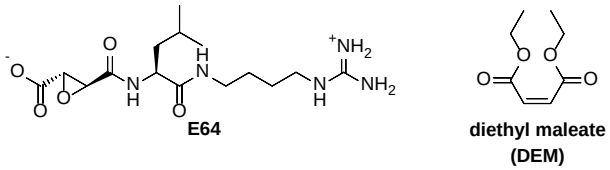

Figure 9: Structures of E64 and DEM, which were used for pharmacological modulation of radiotracer uptake in addition to azadipeptide nitrile **2**

To obtain proof towards cysteine-cathepsin-mediated tumour uptake, the distribution of [^{11}C]**2** was studied by dynamic PET imaging under the administration of non-radioactive **2** as well as the broad-band cysteine peptidase inhibitor E64 and glutathione *S*-reactive agent DEM (Figure 9). The time-activity curves derived from these experiments for various organs are shown in Figure 10. Uptake of [^{11}C]**2** in the presence of unlabelled **2**, i.e. administration of carrier-added (c.a.) radiotracer, was lower than for n.c.a. [^{11}C]**2** over the whole observed time range. Notably, the difference between the uptake of n.c.a. and c.a. radiotracer increased over time. The influence of the radiotracer's lower molar activity is also obvious when the dynamic PET images in Figure 5A and B are compared. This indicates that the uptake of [^{11}C]**2** in the tumour region is at least partially cysteine cathepsin-mediated. Further evidence for target-mediated tumour uptake was obtained by treatment with E64

prior to administration of [^{11}C]**2**. This agent inhibits the cathepsins L, S, B and K[57,58] irreversibly and is stable towards uncatalysed reaction with low-molecular-mass thiols,[57] in contrast to azadipeptide nitrile **2**. Furthermore, E64 is not membrane-permeable and should therefore only block tumour-associated extracellular cysteine cathepsins. As indicated by the time-activity curves in Figure 10A, the tumour uptake of [^{11}C]**2** was significantly reduced in the presence of E64. Compared to radiotracer administration at c.a. level, inhibition was more pronounced in the first 10 min p.i. while at later time points the effect of **2** was stronger. Similar to c.a. [^{11}C]**2**, the influence of E64 is visible by comparing the PET images in Figure 6. Interestingly, comparison of the rescaled images in Figure 6A and B indicates that E64 is influencing more the outer zones of the tumour tissue, while the uptake in the central tumour region is less inhibited. This result is different to the effect observed for **2**, which exhibited homogeneous blocking throughout the tumour tissue. The spatially different influences of azadipeptide nitrile **2** and E64 with regards to inhibition of radiotracer uptake in the tumour can be explained by their differing physicochemical properties. While compound **2** should be sufficiently lipophilic for diffusion across membranes, the zwitterionic structure of E64 (Figure 9) should prevent its unfacilitated membrane permeation. In consequence, the inhibitory effect of E64 should be restricted to extracellular cysteine cathepsins, which are mainly secreted by cells located at the invasive edge of the tumour.[59] To obtain insight into the influence of glutathione conjugate formation on the tumour uptake of [^{11}C]**2**, a PET imaging experiment was performed in an animal that underwent pre-treatment with DEM at high dose. This reagent undergoes glutathione S transferase-catalysed Michael addition by glutathione and its use to deplete the pool of endogenous glutathione has been established.[60,61] As shown in Figure 10A, treatment with DEM resulted in significantly decreased tumour uptake but the difference between the baseline and blocked time-activity curves is reduced with increasing time, in contrast to treatment with **2** and E64. Sound conclusions with regards to the influence of glutathione conjugation on the tumour uptake of [^{11}C]**2** cannot be drawn at this stage because the influence of DEM on the global radiotracer pharmacokinetics has to be taken into consideration, which requires further investigations. Influence of pharmacological intervention by **2**, E64 and DEM on radiotracer uptake in the muscle is much less significant than for the neoplastic tissue, particularly at time points >20 min p.i. (Figure 10B), which provides further evidence towards a cysteine cathepsin-mediated tumour uptake of [^{11}C]**2**. Pharmacological treatment has also less impact on the uptake of [^{11}C]**2** in the brain (Figure 10C). The strongest effect can be observed for compound **2**. Even though its polar character should exclude permeation of the blood-brain barrier, also E64 shows some inhibitory effect on the brain uptake. However, investigations on the brain permeation of this cysteine protease inhibitor have not been reported and a transport facilitated by carriers such as oligopeptide transporters might be possible.[62] Considering that cysteine cathepsins are known to be expressed in the central nervous system, where they are involved in the proteolytic processing of neuropeptide precursors,[63] the observed effects of **2** and E64 might indicate an at least partially target-mediated brain uptake of [^{11}C]**2**. On the other hand, the brain represents an organ of high glutathione content[64] and reaction with glutathione is also responsible for the tissue retention of the blood perfusion tracer ^{99m}Tc-HMPAO.[61,65] The influence of DEM on the brain uptake of [^{11}C]**2** is similar to that on the uptake in the tumour as radiotracer retention is significantly reduced in the early phase while the uptake values at later time points are greater than for the baseline curve. This finding could be interpreted in the way that the uptake of [^{11}C]**2** is determined by perfusion in the early phase while target-mediated uptake prevails at later time points. The impact of the blocking agents on the blood clearance of [^{11}C]**2** is shown in Figure 10D. All three blocking agents reduce the blood levels of the radiotracer to a similar extent. This result can be explained by considering that thiol-reactive functional groups are present in all three agents: an electron-deficient double bond in DEM, an activated epoxide in E64 and a cyano group in azadipeptide nitrile **2**. The thiol reactivity of compound **2** has been discussed above. Similar to DEM, the epoxide group in E64 could react with glutathione catalysed by glutathione *S*-transferase as such a biotransformation has been reported for loxistatin (also known as E64d),[66] which is an E64-related epoxysuccinylated amino acid derivative. The π isoenzyme of glutathione *S*-transferase is expressed at high level in erythrocytes.[67] Therefore, a

glutathione-competitive component might be also present in the pharmacological action of E64 and **2** on the uptake of [^{11}C]**2**.

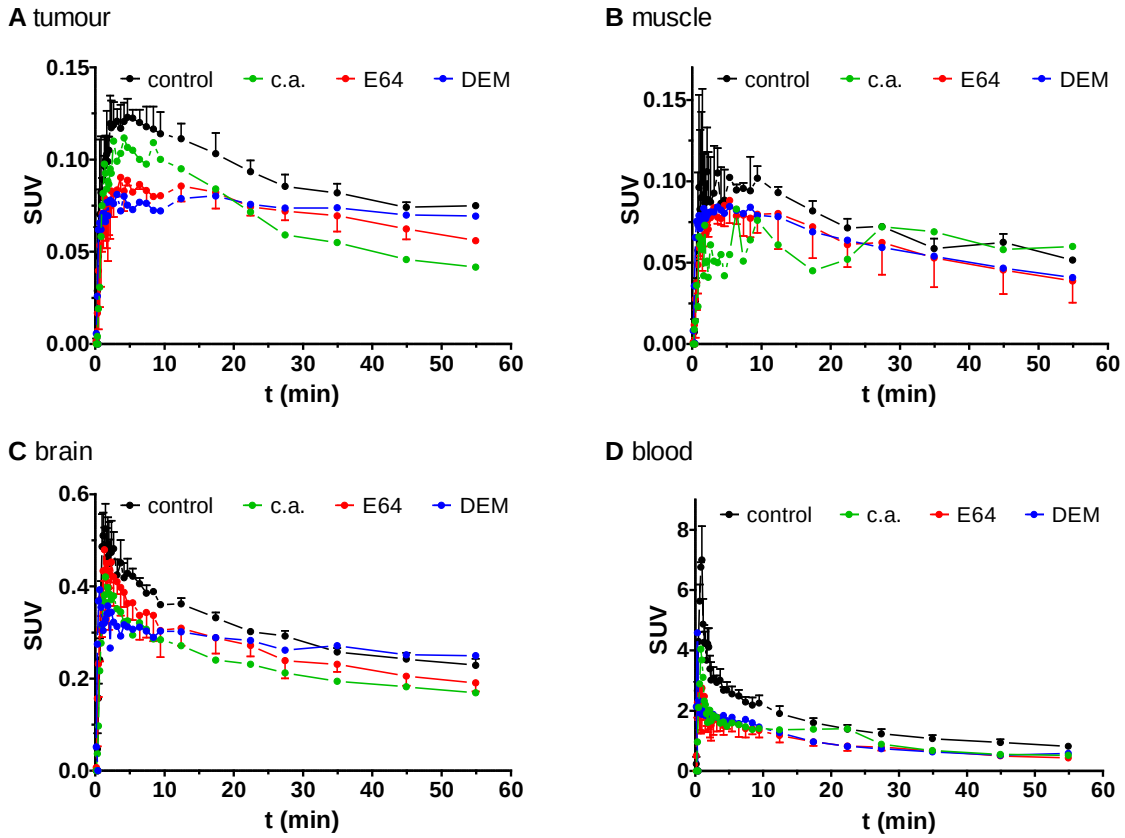

Figure 10: Time-activity curves of [^{11}C]**2** for selected organs in the absence (control; n=6) and presence of **2** (c.a.; 26.6 mg/kg, n=1, respresentative data from one of two experiments are shown), E64 (9.3 mg/kg, n=2) or DEM (567 mg/kg, n=1). Shown are the mean values ± SD.

4. Conclusion

An efficient and reliable radiosynthesis for the ^{11}C-methylation of the cysteine cathepsin-targeting azadipeptide nitrile **1** has been established. Characterisation of the resulting radiotracer [^{11}C]**2** by small-animal PET imaging in tumour xenograft-bearing mice confirmed the complex pharmacokinetic behaviour of its ^{18}F-fluoroethylated counterpart that arises from the inherent thiol reactivity of azadipeptide nitriles. However, pharmacological modulation of the radiotracer uptake by different agents suggests a cysteine cathepsin-mediated tumour uptake, which also allows for positive conclusions towards therapeutic targeting of tumour-associated cysteine cathepsins. This study confirms the limited suitability of cysteine protease inhibitors of the azadipeptide nitrile chemotype as radiotracers for the imaging of cysteine cathepsin in vivo.

5. Acknowledgements

We wish to express our gratitude to Dr. Ralf Bergmann for the dedicated performance of the PET experiments and many fruitful discussions. The excellent technical assistance of Regina Herrlich in the animal experiments is gratefully acknowledged. Furthermore, we are grateful to Stefan Preusche, Norman Dohn and Frank Hobitz for producing [^{11}C]CH_4 at the cyclotron. The authors thank the Helmholtz Association for funding a part of this work through the Helmholtz Cross-Programme Initiative “Technology and Medicine – Adaptive Systems”. RL acknowledges partial financial support by the Fonds der Chemischen Industrie.

5. References

1. Reiser J, Adair B, Reinheckel T. Specialized roles for cysteine cathepsins in health and disease. *J Clin Invest.* 2010;120(10):3421-3431.
2. Patel S, Homaei A, El-Seedi HR, Akhtar N. Cathepsins: Proteases that are vital for survival but can also be fatal. *Biomed Pharmacother.* 2018;105:526-532.
3. Yang M, Zhang Y, Pan J, et al. Cathepsin L activity controls adipogenesis and glucose tolerance. *Nat Cell Biol.* 2007;9(8):970-977.
4. Araujo TF, Cordeiro AV, Vasconcelos DAA, Vitzel KF, Silva VRR. The role of cathepsin B in autophagy during obesity: A systematic review. *Life Sci.* 2018;209:274-281.
5. Liuzzo JP, Petanceska SS, Moscatelli D, Devi LA. Inflammatory mediators regulate cathepsin S in macrophages and microglia: A role in attenuating heparan sulfate interactions. *Mol Med.* 1999;5(5):320-333.
6. Tato M, Kumar SV, Liu Y, et al. Cathepsin S inhibition combines control of systemic and peripheral pathomechanisms of autoimmune tissue injury. *Sci Rep.* 2017;7(1):2775.
7. Stoka V, Turk V, Turk B. Lysosomal cathepsins and their regulation in aging and neurodegeneration. *Ageing Res Rev.* 2016;32:22-37.
8. Liu CL, Guo J, Zhang X, Sukhova GK, Libby P, Shi GP. Cysteine protease cathepsins in cardiovascular disease: from basic research to clinical trials. *Nat Rev Cardiol.* 2018;15(6):351-370.
9. Manchanda M, Das P, Gahlot GPS, et al. Cathepsin L and B as Potential Markers for Liver Fibrosis: Insights From Patients and Experimental Models. *Clin Transl Gastroenterol.* 2017;8(6):e99.
10. Tan GJ, Peng ZK, Lu JP, Tang FQ. Cathepsins mediate tumor metastasis. *World J Biol Chem.* 2013;4(4):91-101.
11. Olson OC, Joyce JA. Cysteine cathepsin proteases: regulators of cancer progression and therapeutic response. *Nat Rev Cancer.* 2015;15(12):712-729.
12. Pogorzelska A, Żołnowska B, Bartoszewski R. Cysteine cathepsins as a prospective target for anticancer therapies-current progress and prospects. *Biochimie.* 2018;151:85-106.
13. Pišlar A, Jewett A, Kos J. Cysteine cathepsins: Their biological and molecular significance in cancer stem cells. *Semin Cancer Biol.* 2018;53:168-177.
14. Lecaille F, Kaleta J, Brömme D. Human and Parasitic Papain-Like Cysteine Proteases: Their Role in Physiology and Pathology and Recent Developments in Inhibitor Design. *Chem Rev.* 2002;102(12):4459-4488.
15. Siklos M, BenAissa M, Thatcher GR. Cysteine proteases as therapeutic targets: does selectivity matter? A systematic review of calpain and cathepsin inhibitors. *Acta Pharm Sin B.* 2015;5(6):506-519.
16. Kramer L, Turk D, Turk B. The Future of Cysteine Cathepsins in Disease Management. *Trends Pharmacol Sci.* 2017;38(10):873-898.
17. Drake MT, Clarke BL, Oursler MJ, Khosla S. Cathepsin K Inhibitors for Osteoporosis: Biology, Potential Clinical Utility, and Lessons Learned. *Endocr Rev.* 2017;38(4):325-350.
18. Löser R, Pietzsch J. Cysteine cathepsins: their role in tumor progression and recent trends in the development of imaging probes. *Front Chem.* 2015;3:37.
19. Rempel BP, Price EW, Phenix CP. Molecular Imaging of Hydrolytic Enzymes Using PET and SPECT. *Mol Imaging.* 2017;16:1536012117717852.
20. Bennacef I, Rubins D, Riffel K, et al. Towards the imaging of Cathepsin K by PET. *J Label Compd Radiopharm.* 2013;56(S1):S49.
21. Rodnick ME, Shao X, Kozloff KM, Scott PJ, Kilbourn MR. Carbon-11 labeled cathepsin K inhibitors: syntheses and preliminary in vivo evaluation. *Nucl Med Biol.* 2014;41(5):384-389.
22. Löser R, Bergmann R, Frizler M, et al. Synthesis and radiopharmacological characterisation of a fluorine-18-labelled azadipeptide nitrile as a potential PET tracer for in vivo imaging of cysteine cathepsins. *ChemMedChem.* 2013;8(8):1330-1344.
23. Ren G, Blum G, Verdoes M, et al. Non-invasive imaging of cysteine cathepsin activity in solid tumors using a ^{64}Cu-labeled activity-based probe. *PLoS One.* 2011;6(11):e28029.

24. Withana NP, Saito T, Ma X, et al. Dual-Modality Activity-Based Probes as Molecular Imaging Agents for Vascular Inflammation. *J Nucl Med.* 2016;57(10):1583-1590.
25. Withana NP, Ma X, McGuire HM, et al. Non-invasive Imaging of Idiopathic Pulmonary Fibrosis Using Cathepsin Protease Probes. *Sci Rep.* 2016;6:19755.
26. Löser R, Frizler M, Schilling K, Gütschow M. Azadipeptide nitriles: highly potent and proteolytically stable inhibitors of papain-like cysteine proteases. *Angew Chem Int Ed Engl.* 2008;47(23):4331-4334.
27. Hess E, Takacs S, Scholten B, Tarkanyi F, Coenen HH, Qaim SM. Excitation function of the $^{18}O(p,n)^{18}F$ nuclear reaction from threshold up to 30 MeV. *Radiochim Acta.* 2001;89:357–362.
28. Miller PW, Long NJ, Vilar R, Gee AD. Synthesis of ^{11}C, ^{18}F, ^{15}O, and ^{13}N radiolabels for positron emission tomography. *Angew Chem Int Ed Engl.* 2008;47(47):8998-9033.
29. Långström B, Karimi F, Watanabe Y. Endogenous compounds labeled with radionuclides of short half-life-some perspectives. *J Label Compd Radiopharm.* 2013;56(3-4):251-262.
30. Ermert J, Coenen HH. Methods for ^{11}C- and ^{18}F-labelling of amino acids and derivatives for positron emission tomography imaging. *J Label Compd Radiopharm.* 2013;56(3-4):225-236.
31. Steinbach J, Mäding P, Füchtner F, Johannsen B. N.C.A. ^{11}C-labelling of benzenoid compounds in ring positions: Synthesis of nitro-[1-^{11}C]benzene and [1-^{11}C]aniline. *J Label Compd Radiopharm.* 1995;36(1):33-41.
32. Pekošak A, Filp U, Poot AJ, Windhorst AD. From Carbon-11-Labeled Amino Acids to Peptides in Positron Emission Tomography: the Synthesis and Clinical Application. *Mol Imaging Biol.* 2018;20(4):510-532.
33. Scott PJ. Methods for the incorporation of carbon-11 to generate radiopharmaceuticals for PET imaging. *Angew Chem Int Ed Engl.* 2009;48(33):6001-6004.
34. Rotstein BH, Liang SH, Placzek MS, et al. ^{11}C=O bonds made easily for positron emission tomography radiopharmaceuticals. *Chem Soc Rev.* 2016;45(17):4708-4726.
35. Dahl K, Halldin C, Schou M. New methodologies for the preparation of carbon-11 labeled radiopharmaceuticals. *Clin Transl Imaging.* 2017;5(3):275-289.
36. Taddei C, Gee AD. Recent progress in [^{11}C]carbon dioxide ([^{11}C]CO_2) and [^{11}C]carbon monoxide ([^{11}C]CO) chemistry. *J Label Compd Radiopharm.* 2018;61(3):237-251.
37. Wilson TC, Cailly T, Gouverneur V. Boron reagents for divergent radiochemistry. *Chem Soc Rev.* 2018;47(18):6990-7005.
38. Wuest F, Berndt M, Kniess T. Carbon-11 Labeling Chemistry Based upon [^{11}C]Methyl Iodide. In: Schubiger PA, Lehmann L, Friebe M, eds. *PET Chemistry - The Driving Force in Molecular Imaging.* Berlin Heidelberg: Springer-Verlag; 2007.
39. Antoni G. Development of carbon-11 labelled PET tracers-radiochemical and technological challenges in a historic perspective. *J Label Compd Radiopharm.* 2015;58(3):65-72.
40. Kniess T, Laube M, Brust P, Steinbach J. 2-[^{18}F]Fluoroethyl tosylate – a versatile tool for building ^{18}F-based radiotracers for positron emission tomography. *MedChemComm.* 2015;6(10):1714-1754.
41. Boscutti G, Huiban M, Passchier J. Use of carbon-11 labelled tool compounds in support of drug development. *Drug Discov Today Technol.* 2017;25:3-10.
42. Windhorst AD, Poot AJ, Vugts DJ. Carbon-11 chemistry. Why fighting 20 minutes half-life really makes sense. In: Aboagye, E., Aigbirhio F, Allott L, et al. Abstracts of the 26th international isotope society (UK group) symposium: Synthesis & applications of labelled compounds 2017. *J Label Compd Radiopharm.* 2018;61:1115-1130.
43. Frizler M, Lohr F, Furtmann N, Kläs J, Gütschow M. Structural Optimization of Azadipeptide Nitriles Strongly Increases Association Rates and Allows the Development of Selective Cathepsin Inhibitors. *J Med Chem.* 2011;54(1):396-400.
44. Kuchar M, Neuber C, Belter B, et al. Evaluation of fluorine-18-labelled a1(I)-N-telopeptide analogs as substrate-based radiotracers for PET imaging of melanoma-associated lysyl oxidase. *Front Chem.* 2018;6:121.
45. Loureiro LR, Feldmann A, Bergmann R, et al. Development of a novel target module redirecting UniCAR T cells to Sialyl Tn-expressing tumor cells. *Blood Cancer J.* 2018;8(9):81.

46. Wolf S, Haase-Kohn C, Lenk J, et al. Expression, purification and fluorine-18 radiolabeling of recombinant S100A4: a potential probe for molecular imaging of receptor for advanced glycation endproducts in vivo? *Amino Acids.* 2011;41(4):809-820.
47. Pietzsch J, Bergmann R, Wuest F, Pawelke B, Hultsch C, van den Hoff J. Catabolism of native and oxidized low density lipoproteins: in vivo insights from small animal positron emission tomography studies. *Amino Acids.* 2005;29(4):389-404.
48. Heidelberger C, Guggisberg A, Stephanon E, Hesse M. Amidine als Zwischenprodukte bei Umamidierungsreaktionen. 9. Mitteilung über Umamidierungsreaktionen. *Helv Chim Acta.* 1981;64(2):399-406.
49. Eriksson J, Van Kooij R, Schuit RC, et al. Synthesis of [3-N-^{11}C-methyl]temozolomide via in situ activation of 3-N-hydroxymethyl temozolomide and alkylation with [^{11}C]methyl iodide. *J Label Compd Radiopharm.* 2015;58(3):122-126.
50. Vidal B, Karpenko IA, Liger F, et al. [^{11}C]PF-3274167 as a PET radiotracer of oxytocin receptors: Radiosynthesis and evaluation in rat brain. *Nucl Med Biol.* 2017;55:1-6.
51. Malmquist J, Varnäs K, Svedberg M, et al. Discovery of a Novel Muscarinic Receptor PET Radioligand with Rapid Kinetics in the Monkey Brain. *ACS Chem Neurosci.* 2018;9(2):224-229.
52. Vraka C, Nics L, Wagner KH, Hacker M, Wadsak W, Mitterhauser M. LogP, a yesterday's value? *Nucl Med Biol.* 2017;50:1-10.
53. Ishibashi O, Mori Y, Kurokawa T, Kumegawa M. Breast cancer cells express cathepsins B and L but not cathepsins K or H. *Cancer Biochem Biophys.* 1999;17(1-2):69-78.
54. Tsai JY, Lee MJ, Chang MD, Wang HC, Lin CC, Huang H. Effects of novel human cathepsin S inhibitors on cell migration in human cancer cells. *J Enzyme Inhib Med Chem.* 2014;29(4):538-546.
55. Swisher LZ, Prior AM, Gunaratna MJ, et al. Quantitative electrochemical detection of cathepsin B activity in breast cancer cell lysates using carbon nanofiber nanoelectrode arrays toward identification of cancer formation. *Nanomed-Nanotechnol.* 2015;11(7):1695-1704.
56. Uhlman A, Folkers K, Liston J, Pancholi H, Hinton A. Effects of Vacuolar H^+-ATPase Inhibition on Activation of Cathepsin B and Cathepsin L Secreted from MDA-MB231 Breast Cancer Cells. *Cancer Microenviron.* 2017;10(1-3):49-56.
57. Powers JC, Asgian JL, Ekici OD, James KE. Irreversible inhibitors of serine, cysteine, and threonine proteases. *Chem Rev.* 2002;102(12):4639-4750.
58. Bossard MJ, Tomaszek TA, Thompson SK, et al. Proteolytic Activity of Human Osteoclast Cathepsin K. *J Biol Chem.* 1996;271(21):12517-12524.
59. Strojnik T, Kos J, Židanik B, Golouh R, Lah T. Cathepsin B Immunohistochemical Staining in Tumor and Endothelial Cells Is a New Prognostic Factor for Survival in Patients with Brain Tumors. *Clin Cancer Res.* 1999;5(3):559-567.
60. Plummer JL, Smith BR, Sies H, Bend JR. Chemical depletion of glutathione in vivo. *Methods Enzymol.* 1981;77:50-59.
61. Sasaki T, Senda M. Technetium-99m-meso-HMPAO as a potential agent to image cerebral glutathione content. *J Nucl Med.* 1997;38(7):1125-1129.
62. Keep RF, Smith DE. Oligopeptide Transport at the Blood-Brain and Blood-CSF Barriers. In: Kasta AJ, ed. *Handbook of Biologically Active Peptides.* Amsterdam: Academic Press; 2006:1423-1428.
63. Hook V, Funkelstein L, Wegrzyn J, Bark S, Kindy M, Hook G. Cysteine Cathepsins in the secretory vesicle produce active peptides: Cathepsin L generates peptide neurotransmitters and cathepsin B produces beta-amyloid of Alzheimer's disease. *Biochim Biophys Acta.* 2012;1824(1):89-104.
64. Griffith OW, Meister A. Glutathione: interorgan translocation, turnover, and metabolism. *Proc Natl Acad Sci USA.* 1979;76(11):5606-5610.
65. Audi SH, Roerig DL, Haworth ST, Clough AV. Role of glutathione in lung retention of ^{99m}Tc-hexamethylpropyleneamine oxime in two unique rat models of hyperoxic lung injury. *J Appl Physiol (1985).* 2012;113(4):658-665.
66. Fukushima K, Arai M, Ogawa H, Suwa T, Satoh T. Identification of glutathione conjugate formed from loxistatin in rats. *Xenobiotica.* 1989;19(5):521-529.

67. Awasthi Y, Sharam R, Singhal SS. Human Glutathione *S*-transferases. *Int J Biochem.* 1994;26(3):295-308.